Letters in Applied NanoBioScience
Open-Access Journal (ISSN: 2284-6808)

Article
Volume 14, Issue 1, 2025, 26
https://doi.org/10.33263/LIANBS141.026

In Silico Identification of New Anti-SARS-CoV-2 Main Protease (M^{pro}) Compounds from *Datura fastuosa*

Reese Ru En Tien [1], Yin-Quan Tang [1,2,*]

[1] School of Biosciences, Faculty of Health and Medical Sciences Taylor's University, 47500 Subang Jaya 47500, Malaysia
[2] Digital Health and Medical Advancement Impact Lab, Taylor's University, 47500 Subang Jaya, Malaysia
* Correspondence: yinquan.tang@taylors.edu.my (Y.-Q.T)

Scopus Author ID 36769481900
Received: 3.10.2023; Accepted: 7.07.2024; Published: 24.09.2024

Abstract: SARS-CoV-2 main protease (M^{pro}) plays a crucial role in regulating the viral life cycle, making it an attractive target for anti-COVID-19 therapies. The rapid development of novel therapeutic compounds is crucial; unfortunately, traditional drug development methods are time-consuming and expensive. In this study, we present the first report on identifying potential anti-COVID-19 agents from *Datura fastuosa* that inhibit SARS-CoV-2 main protease (M^{pro}) using a bioinformatics and computational biology approach. A library of eighteen bioactive compounds in *D. fatuosa* was created from the PubChem database. Molecular docking studies were performed by targeting M^{pro} (PDB ID: 6lu7) via Discovery Studio Visualizer and PyRx platform. Top hits compounds were selected to study their ADMET properties and drug-likeness properties using the pkCSM pharmacokinetics tool to understand the stability, interaction, conformational changes, and pharmaceutical-relevant parameters. Six exclusive bioactive compounds, namely, daturataturin A (-8.6 kcal/mol), daturametelin J (-8.6 kcal/mol), baimantuoluoside B (-8.5 kcal/mol), 12-deoxywithastramonolide (-8.4 kcal/mol), baimantuoluoside A (-7.9 kcal/mol) and daturaolone (-7.6 kcal/mol) showed stronger inhibitory activity against Mpro of SARS-CoV-2, than N3 inhibitor (positive control) (-7.4 kcal/mol). However, further modification is needed to improve their bioavailability based on these compounds' ADMET and drug-likeness studies. From these results, it was concluded exclusive compounds from *D.fastuosa* (daturataturin A, daturametelin J, baimantuoluoside A, baimantuoluoside B, 12-deoxywithastramonolide, daturaolone, daturadiol, and daturataurin B) possess potential therapeutic properties against COVID-19.

Keywords: computational screening; coronavirus disease; molecular docking; severe acute respiratory syndrome coronavirus 2; main protease.

1. Introduction

A novel virus strain, SARS-CoV-2 (severe acute respiratory syndrome coronavirus 2), is the causative agent of the coronavirus disease (COVID-19) that emerged in late 2019 [1]. The global spread of SARS-CoV-2 to more than 203 countries led the World Health Organization to declare a pandemic on 12 March 2020 [2]. As of February 2022, the global count of SARS-CoV-2 infections surpassed 400 million, leading to an estimated 5.8 million deaths [1]. Respiratory droplet transmission is the main transmission route and can also be transmitted through person-to-person contact and aerial droplets. Most patients infected with SARS-CoV-2 have symptoms such as fever, cough, and fatigue. Globally, as of 29 March 2023,

there have been 761,402,282 confirmed cases of COVID-19, including 6,887,000 deaths, reported to WHO [3].

Proteases play a crucial role in coronaviruses, making them one of the best-studied proteins in coronavirus. M^{pro}, also known as $3CL^{pro}$, is the main protease for viral replication by regulating the proteolytic processing of the replicase polyprotein (pp1a and pp1ab) [4]. Inhibition of this viral protease enzyme blocks the M^{pro} activity as it will block the viral replication, thus diminishing the illness's spread. Liu et al. [5] suggested that the M^{pro} is a potential drug target to inhibit SARS-Cov-2 replication due to its highly conserved sequence at the binding pocket and availability of 3D structure, compared to spike proteins which have high mutation rates at its receptor binding motif [1,6]. In addition, Zhang et al. [7] suggested that inhibitors that target M^{pro} are unlikely toxic since there is no known similar cleavage specificity among the human proteases.

Despite the successful development of COVID-19 vaccines to protect vaccinated individuals from infection, the emergence of SARS-CoV-2 variants with mutated variants has led to resistance against the immunity induced by vaccines. The limitation of vaccines highlights the need for developing new drugs that can be taken orally as a complementary approach alongside vaccines [1]. In addition, despite many repurposed antiviral drugs that have been discovered as COVID-19 drugs, these drugs result in unfavorable side effects that make them unsuitable for use in the general population [2]. Thus, research has been focusing on finding an alternative natural product that has the potential to be developed as an anti-covid drug with fewer side effects.

In the present research, we have chosen *Datura fastuosa*, a wild weed belonging to the family Solanaceae. It originated from the West Indies or America and is now distributed in tropical regions. Many pharmacological studies of *D. fastuosa* showed that it possessed antimicrobial, anti-inflammatory, analgesic, neurological, and healing effects [8]. However, the potency of *D. fastuosa* against SARS-CoV-2 remains unclear. This will be the first report investigating the anti-covid properties of *D. fastuosa* compounds. We hope this study will be one of the contributing factors for drug development targeting M^{pro} of SARS-COV-2.

2. Materials and Methods

2.1. Protein retrieval and preparation.

The main target for this study is SARS-CoV-2' M^{pro}. The three-dimensional structure of M^{pro} in complex with an inhibitor N3 (PDB ID: 6lu7, chain A, 2.16 Å) was obtained from Protein Data Bank (www.rcsb.org). The ligand N3 was used as a positive control. The retrieved 3D M^{pro} structure was prepared using BIOVIA Discovery Studio Visualizer to remove water, heteroatoms and N3 ligand molecules to reveal the active site of M^{pro} which are His41, Met49 Phe140, Gly143, His164, Met165, Glu166, Leu167, Pro168, His172, Gln189, Thr190, and Ala191 as shown in Figure 1.

2.2. Ligand preparation.

A library of 18 compounds of *D. fastuosa* was selected based on a study that examined the chemical constituents of the plants using phytochemical analysis [8]. The 18 compounds were retrieved from the PubChem database in SDF formats as 3D conformers (Table 1). Before the molecular docking was performed, energy minimization was performed for all ligands, which were saved in PDBQT format using OpenBabel in the PyRx program.

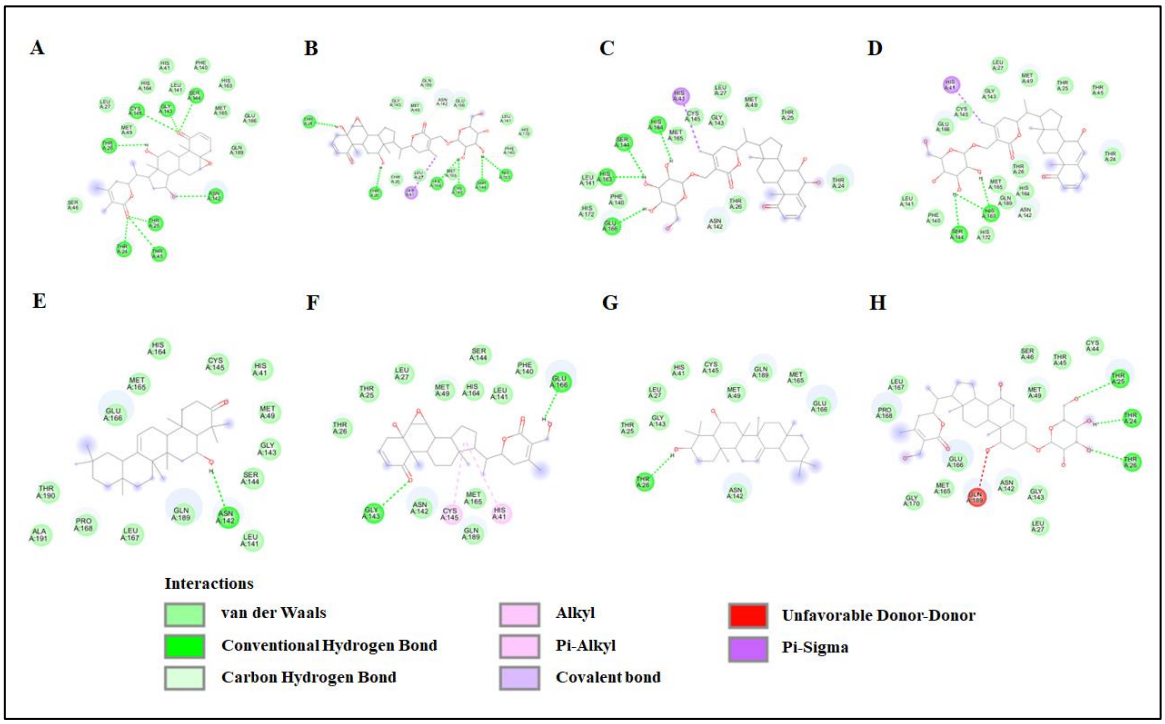

Figure 1. 2D Diagrams of interaction of active site of M^{pro} with N3 inhibitor.

Table 1. Library of 18 selected compounds from *Datura fastuosa.*

No.	Ligand name	Pubchem CID
1	Baimantuoluoside B	101482745
2	Vanillin	1183
3	Daturataturin A	14825627
4	Trifluoro-, 2,2- dimethyl propyl ester	15696281
5	Acetic acid	176
6	Cis-2- nitro-4-t-butyl cyclohexanone	21680401
7	Daturadiol	3084830
8	12-deoxywithastramonolide	44576309
9	Scopoletin	5280460
10	Isofraxidin	5318565
11	4-trifluoro acetoxy octane	549895
12	Daturametelin J	102139051
13	Baimantuoluoside A	101434809
14	Daturataurin B	14825632
15	Aposcopolamine	3083622
16	Daturine	154417
17	Daturaolone	122859
18	Scopolamine	3000322

2.3. Molecular docking.

Molecular docking was performed using PyRx program (Python Prescription 0.8) by Vina Wizard as the engine for Autodock Vina v.1.2.0. The grid box was set to surround the active site of M^{pro} which was centered at X= -20.8561, Y= 13.6293, Z= 68.5284 with dimensions (Å) X= 23.0224, Y= 28.5139, Z= 28.7321. The results of the binding analysis and the best model for each protein-ligand interaction were saved. The BIOVIA Discovery Studio Visualizer was used to visualize the 3D and 2D binding conformation diagrams.

2.4. Drug-likeness prediction.

The ligands were examined based on Lipinski's five rules, which include (a) molecular mass, (b) degree of lipophilicity (Log P), (c) hydrogen bond donors, (d) hydrogen bond acceptors, and (e) rotatable bond. According to Lipinski's rule of five, a drug compound

demonstrates favorable characteristics such as effective membrane permeability, high oral bioavailability, and efficient absorption in the gastrointestinal tract of humans. The structures of the compound present in *D. fastuosa* were obtained from the PubChem database in canonical SMILE files for ADMET (Absorption, Distribution, Metabolism, Excretion, and Toxicity) analysis using pkCSM (https://biosig.lab.uq.edu.au/pkcsm/). Compounds with higher binding affinity than the positive control, N3, were then selected for drug-likeness using Lipinski's rule of five. With respect to the criteria, molecular weight (MW) < 500, the number of hydrogen bond acceptors <- 10, the number of hydrogen bond donors <- 5, and the Log Po/w <- 5, no more than 1 violation is allowed [9].

3. Results and Discussion

Until today, the SARS-CoV-2 infection is still widespread. Although different combinations of antiviral drugs are practiced in some countries, synthetic-based antiviral drugs bring adverse side effects to the human body. For instance, ritonavir is a CTP3A inhibitor, leading to elevated plasma concentrations of drugs primarily metabolized by CYP3A [1]. Therefore, researchers worldwide are actively seeking natural compounds that can serve as highly effective therapeutic candidates against COVID-19 while minimizing potential side effects.

This research was conducted on a medicinal plant, *D. fastuosa*, and its compounds that might potentially inhibit M^{pro} of SARS-CoV-2. M^{pro} functions to cleave host polyproteins and induce the formation of protein for viral replication [10]. Therefore, it is possible that selected compounds of *D. fastuosa* in the study can be used in drug development to inhibit viral infection, as our docking results showed relatively good binding affinity of the compounds to M^{pro}.

3.1. Molecular docking studies.

After successfully docking selected ligands into the active site of SARS-CoV-2 M^{pro}, Vina Wizard produced various modes of ligand-protein interactions with a particular docking score (binding energy), as illustrated in Figure 2. The binding mode with the least binding energy is the most stable for the ligand and, hence, is regarded as the best binding mode. Compounds possessing a binding affinity energy score of -7.4 or even less are considered more suitable for effectively inhibiting COVID-19. Based on Table 2, 8 out of 18 tested ligands of *D. fastuosa* were found to have higher binding affinity than the positive control, N3. It refers to the aim of this study that the bioactive compounds that show higher binding affinity than N3 are predicted to have the ability to inhibit M^{pro}. The lower binding affinity energy means that the ligand-protein complex has a higher tendency to form constant temperature and pressure [11]. Meanwhile, the binding affinity energy of the other compounds is higher than that of the positive control. It was assumed that these compounds were not effective for drug development.

The daturataturin A and daturametelin J had the highest binding scores (-8.6 kcal/mol), followed by the very similar affinity of baimantuoluoside B (-8.5 kcal/mol) and 12-deoxywithastramonolide (-8.4 kcal/mol). Furthermore, the 2 ligands, namely daturadiol and daturataurin B, were found to have the same binding affinity as N3. The best binding modes and corresponding binding affinities are summarized and ranked based on their binding affinities in Table 2.

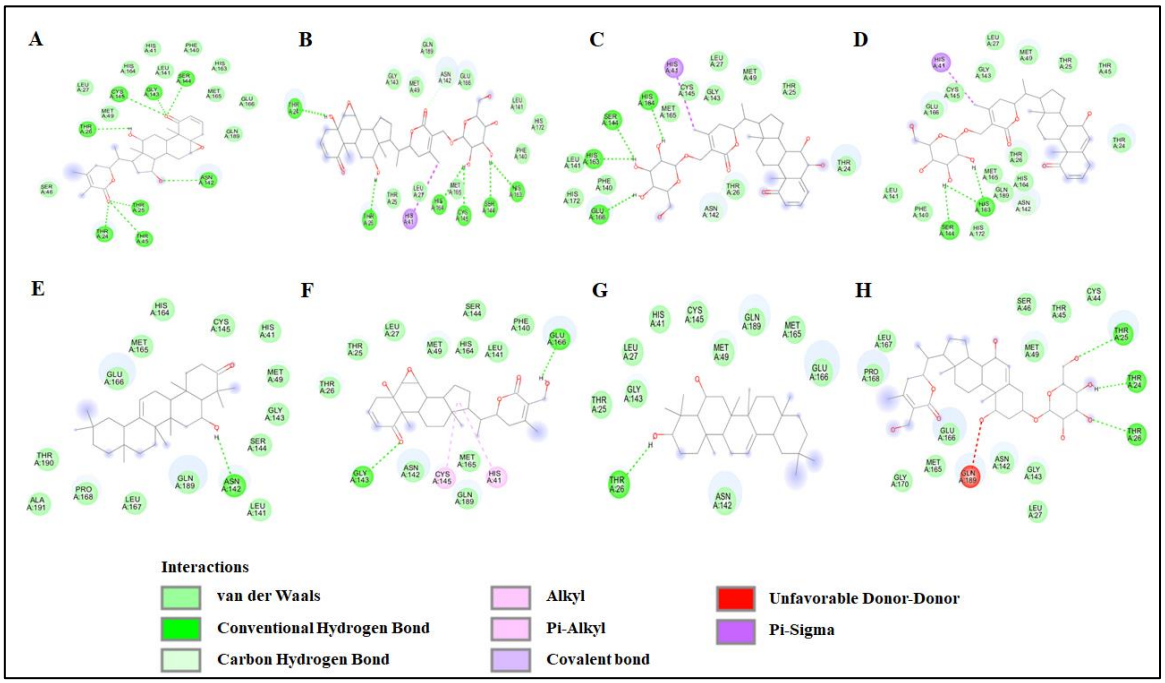

Figure 2. 2D diagrams of *D. fastuosa* compounds interaction with SARS-CoV-2 M^{pro} active site: **(a)** Baimantuoluoside A; **(b)** Baimantuoloside B; **(c)** Daturametelin J; **(d)** Daturataturin A; **(e)** Daturaolone; **(f)** 12-deoxywithstramonoslide; **(g)** Daturadiol; **(h)** Daturataurin B.

The daturataturin A and daturametelin J had the highest binding scores (-8.6 kcal/mol), followed by the very similar affinity of baimantuoluoside B (-8.5 kcal/mol) and 12-deoxywithastramonolide (-8.4 kcal/mol). Furthermore, the 2 ligands, namely daturadiol and daturataurin B, were found to have the same binding affinity as N3. The best binding modes and corresponding binding affinities are summarized and ranked based on their binding affinities in Table 2.

Table 2. Interactions of COVID-19 Main Protease (6lu7) amino acid residues with ligands at receptor sites.

No	Ligand name	Binding affinity energy (kcal/mol)	Interactions with M^{pro} residues		Total number of interactions		
			Hydrogen bond	Hydrophobic interaction	Hydrogen bond	Hydrophobic interaction	Van der Waals
1	daturataturin A	-8.6	Asn142, **Ser144**, His163,	**His41**	4	1	16
2	daturametelin J	-8.6	Asn142**, Ser144**, His163, His164, Glu166	**His41**	5	1	12
3	baimantuoluoside B	-8.5	Thr24, Thr26 Asn142, **Ser144**, Cys145, His163, His164	**His41**	8	1	10
4.	12-deoxywithastramonolide	-8.4	Gly143, Glu166	Cys145**, His41**	2	2	11
5	baimantuoluoside A	-7.9	Thr24, Thr25, Thr45, Asn142, Gly143, **Ser144**, Cys145, Thr26	-	8	-	11
6	daturaolone	-7.6	Asn142	-	1	-	14
7	daturadiol	-7.4	Thr26	-	1	-	10
8	daturataurin B	-7.4	Thr24, Thr25, Thr26	-	3	-	12

No	Ligand name	Binding affinity energy (kcal/mol)	Interactions with M^{pro} residues		Total number of interactions		
			Hydrogen bond	Hydrophobic interaction	Hydrogen bond	Hydrophobic interaction	Van der Waals
9	N3 inhibitor	-7.4	**Phe140, Gly143, Ser144, His164, Glu166, His172, Gln189, Thr190,**	**His41, Met49, Met165, Leu167, Pro 168, Ala191**	9	7	13
10	Aposcopolamine	-6.7	Phe140, Ser144	His41, Met49	2	2	12
11	Isofraxidin	-6.6	Phe140, Leu141, Gly143, Ser144, Cys145, Glu166	His41, Cys145, His163	6	3	7
12	Scopolamine	-6.3	His41, Cys145, Glu166, Met165	His41, Met165	4	2	10
13	daturine	-6.3	Gly143, Ser144, Cys145, Leu141	Leu27	6	1	10
14	Scopoletin	-5.8	Leu141, Gly143, Ser144, Cys145, Glu166,	His41, Cys145	7	2	6
15	cis-2- nitro 4-t-butyl cyclohexanone	-4.9	Ser144, Cys145, Glu166	-	3	-	8
16	vanillin	-4.9	Gly143, Ser144, Gly166	Cys145	5	1	4
17	2,2-Dimethylpropyl Ester	-4.7	Tyr24, His164, Arg188, Gln189	-	4	0	0
18	4-trifluoroacetoxy octane	-4.4	Phe140, Leu141, Gly143, Ser144, Glu166	His41, Cys145, His163	6	3	0
19	Acetic acid	-3	Gly143, Ser144	-	2	0	4

3.2. Molecular interaction studies.

The outcomes of the rigid docking analysis were visualized using BIOVIA Discovery Studios to assess the interactions through 2D (Figure 2) and 3D (Figure 3) diagrams. The number of non-covalent interactions, such as hydrogen bonds, hydrophobic bonds, and van der Waals, are tabulated in Table 2. Among the protein complexes, daturataturin A and daturametelin J strongly correlate with the main protease (6lu7). The main protease with daturataturin A complex formed four hydrogen bonds, i.e., Asn142, Ser144, His163, and one amino acid is involved in forming hydrophobic interaction, i.e., His41. Daturametelin J, on the other hand, forms 5 hydrogen bonds with the main protease, i.e., Asn142, Ser144, His163, His164, Glu166, and one amino acid is involved in the formation of hydrophobic interaction, i.e., His41.

The 8 ligands were selected for viewing the 2D and 3D diagrams to analyze the interaction, which assisted in forming a stable docked complex. All the selected ligands showed significant placement in the active site of SARS-CoV-2' M^{pro} and shared some common residues. The active site of the M^{pro} has a Cys145-His41 catalytic dyad, which is responsible for the cleavage of SARS-CoV-2 polyproteins [12]. Therefore, His-41 and Cys145 are crucial target amino acid residues for inhibition. All 8 compounds are observed to interact with His41 and or Cys145 through hydrogen bonds, hydrophobic bonds, and van der Waals forces, as illustrated in the 2D diagrams (Figure 2). This indicates that these compounds show promising ability to inhibit M^{pro}.

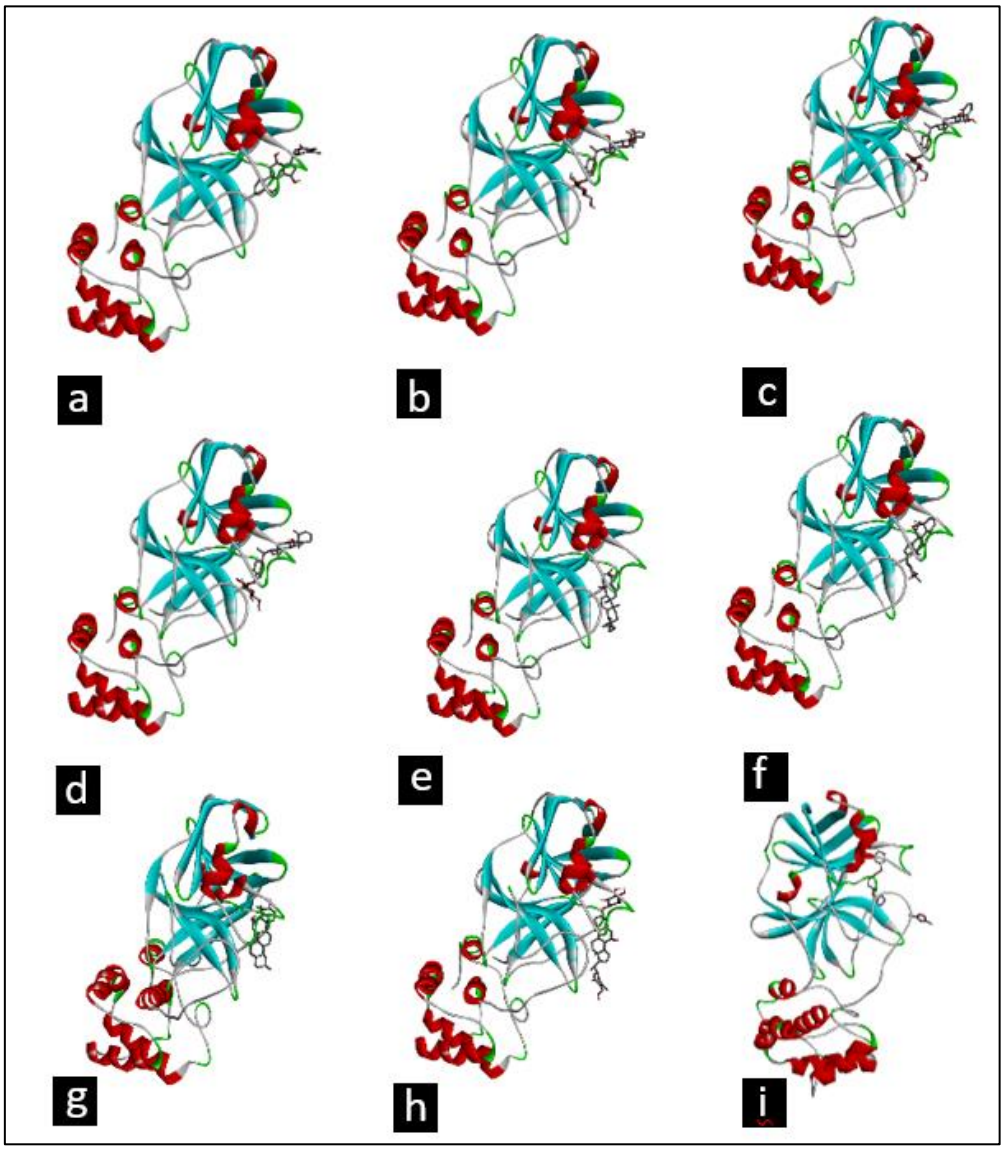

Figure 3. 3D diagrams of *Datura fastuosa* compounds interaction with SARS-CoV-2 M^{pro} active site: **(a)** Baimantuoluoside A; **(b)** Baimantuoloside B; **(c)** Daturametelin J; **(d)** Daturaturin A; **(e)** Daturaolone; **(f)** 12-deoxywithstramonolide; **(g)** Daturadiol; **(h)** Daturataurin B; **(i)** N3 inhibitor.

The binding affinity between ligands and proteins is influenced by non-covalent intermolecular interactions such as hydrogen bonding, hydrophobic, and van der Waals forces between the two molecules [13]. Daturaturin A, having the greatest binding affinity with M^{pro}, has four hydrogen bonds interacting with the active sites of M^{pro} at the residues Asn142, Ser144, and His163. The formation of hydrogen bonds is crucial for stabilizing the ligand-protein interactions. Besides hydrogen bonds, daturataturin A interacts with His41 through a Pi-sigma bond, a type of hydrophobic bond. The existence of hydrophobic bonding further enhances the binding affinity at protein-ligand interfaces through interactions between hydrophobic amino acids and polar solvents [14,15]. Patil et al. [14] stated that the increase in the number of hydrophobic atoms in the active site of the drug-target interface can further increase the biological activity of the drug lead. Other types of hydrophobic bonds also include alkyl, pi-alky, and pi-sigma. Hydrophobic interactions can increase the binding affinity between target-drug interfaces. Increasing the number of hydrophobic atoms in the drug-target interface's active core further increases the drug lead's biological activity [16].

Hydrogen bonds play a crucial role in enhancing the stability of protein-ligand binding interactions in both docking complexes. These networks of hydrogen bonds positively impact

the binding between the protein and ligand [17]. Daturataturin A, daturametelin J, and baimantuoluoside B exhibit two types of hydrogen bonds: conventional and carbon-hydrogen. The carbon-hydrogen bond (CHO) is relatively weaker compared to the conventional hydrogen bonds (NH…O, OH…O, OH…N, and NH…N) due to the longer average distance between the atoms involved in CHO interactions. It was found that the carbon-hydrogen bond is responsible for the process of molecular recognition [18,19].

3.3. Drug likeliness.

Drug-likeness properties were analyzed using Lipinski's rule of Five. According to Lipinski's rule of five, a molecule is predicted to have favorable characteristics such as good oral bioavailability, efficient membrane permeability, and strong absorption in the human while its log p ≤ 5; molecular weight ≤ 500 Dalton; H-bond acceptor ≤10 and H-bond donor ≤5 [20]. In our study, 4 compounds, i.e., baimantuoluoside A, baimantuoluoside B daturametelin J and daturataurin B violated more than one rule. However, there is an exception to Lipinski's rule for natural products. It is believed that this is due to evolutionary selection that determines special chemical structures of natural compounds [20]. Therefore, these four compounds can still be acceptable as drug-likeness compounds. However, the four compounds with molecular weight values of more than 500.000 Dalton were estimated to be unable to pass membrane cells. Therefore, an advanced study is required to make molecular weight smaller than 500.000 Dalton.

Eight compounds with higher or the same binding affinity as N3 were chosen to predict their drug likeliness using Lipinski's rule of five, which aids in differentiating between drug-like and non-drug-like particles based on their vital atomic characteristics [21]. Based on Table 3, four compounds were found to obey Lipinski's rule of five, and another half did not obey the rule. Baimantuoluoside A, baimantuoluoside B, daturametelin J, and daturataurin B show higher molecular weight, H-bond donor, and H-bond acceptor.

Both daturadiol and daturaolone are predicted with log P higher than 5. The log P value is a measure of a molecule's solvability in water or fat and falls within a range of -0.4 to 5. A higher log P value indicates that a molecule has more hydrophobic characteristics, which can lead to increased toxicity levels. This is because hydrophobic molecules tend to remain disconnected in the lipid bilayer membrane for longer periods and can spread more widely throughout the body. As a result, the molecule's ability to selectively inhibit the target protein, M^{pro}, may be reduced. Conversely, a more negative log P value indicates that the molecule is less permeable [11].

Table 3. Physiochemical properties of potential bioactive compounds from *D. fastuosa*. Values highlighted in bold represent those that fall outside the desired range of each parameter.

	Drug-like properties (Lipinski's rule of five)					
Compounds	**Molecular weight (≤ 500 Da)**	**Log P (≤ 5)**	**H-bond donor (≤ 5)**	**H-bond acceptor (≤10)**	**Rotatable bond (≤ 10)**	**Violations**
12-deoxywithastramonolide	470.6060	3.3529	2	6	3	0
baimantuoluoside A	**648.746**	0.1479	**6**	**12**	6	3
baimantuoluoside B	**648.746**	0.1479	**6**	**12**	6	3
daturadiol	442.728	**7.1397**	2	2	0	1
daturametelin J	**632.747**	0.9367	**6**	**11**	6	3
daturaolone	440.712	**7.3479**	1	2	0	1
daturataturin A	**616. 748**	1.9659	5	10	6	1
daturaturin B	**636.779**	0.9525	**7**	**11**	6	3

3.4. ADMET evaluation.

The utilization of ADMET analysis in the early stages of drug discovery is beneficial as it minimizes the occurrence of significant clinical trial failures [22]. Thus, it saves enormous cost and time. The 8 compounds are subjected to ADMET analysis. Water solubility, Caco-2 permeability, human intestinal absorption, and skin permeability are essential parameters related to absorption in the process of drug development [23]. Results showed that the water solubility of all compounds, except daturaolone and daturadiol, is high as they are higher than -6 log moL/L. The predicted low water solubility of daturadiol and daturaolone may be due to their predicted higher log P values, 7.1397 and 7.3479, respectively. A log P value higher than 5 suggests that a compound has a higher affinity for the lipid solvent phase, suggesting poor water solubility. The poor water solubility of the drugs might decrease the desired concentration of drugs in systemic circulation for achieving pharmacological response as fewer drugs will be dissolved in the aqueous gastrointestinal fluids and thus cause insufficient bioavailability [24]. Despite having poor aqueous solubility, Pouton [25] shows that poorly water-soluble drugs can still be successfully formulated for oral administration through methods such as particle size reduction to ensure consistent bioavailability. The Vdss, fraction unbound, BBB membrane, and CNS permeability were used to study drug distribution [26]. All compounds are predicted to have a low value of Vdss, possibly due to these compounds being more likely bound to plasma proteins, as predicted by the fraction unbound. This means that a higher dose of the drug is required to achieve a given plasma concentration. Moving on, a negative AMES toxicity test means that all compounds are non-mutagenic and non-carcinogenic. Even though 6 compounds are predicted as hERG II inhibitors, further studies and evaluations can help determine their potential as viable drug candidates.

The ADMET properties of all 8 ligands were evaluated using pkCSM. Based on Table 4, all the compounds exhibit favorable intestinal absorption, with daturaolone displaying the highest absorption percentage (95.60%), followed by daturadiol (94.34%). All the compounds were AMES negative. A skin permeability value greater than -2.5 cm/h shows low skin permeability, and all compounds exhibited high skin permeability with values less than -3.5 log Kp. Two out of eight drug compounds (daturaolone and daturadiol) had high Caco-2 permeability (>0.90 cm/s).

Table 4. ADMET properties of selected Datura fastuosa compounds showed higher binding affinity than N3.

Parameters/ models	Datura o-lone	Datura-taturin A	Daturadiol	12-deoxywithastramonolide	Datura-metelin J	Baimantuoluoside A	Datura-taurin B	Baimantuoluoside B
Water solubility (log mol/L)	-6.757	-4.454	-6.566	-4.983	-4.14	-3.949	-3.758	-3.949
Caco2 permeability (log Papp in 10^-6 cm/s)	1.333	0.378	1.223	0.826	0.412	0.574	0.424	0.574
Intestinal Absorption (human)	95.592	58.526	94.341	85.412	44.73	39.149	43.17	39.49
Skin Permeability (log Kp)	-3.082	-2.748	-3.151	-3.211	-2.739	-2.736	-2.736	-2.736
P-glycoprotein substrate	No	Yes	Yes	Yes	Yes	Yes	Yes	Yes
P-glycoprotein I inhibitior	Yes	Yes	Yes	Yes	Yes	Yes	Yes	Yes

Parameters/ models	Daturao-lone	Datura-taturin A	Daturadiol	12-deoxywithastramonolide	Datura-metelin J	Baimantuoluoside A	Datura-taurin B	Baimantuoluoside B
P-glycoprotein II inhibitior	Yes	No	Yes	Yes	No	No	No	No
VDss (log L/kg)	0.303	-0.774	0.279	-0.211	-0.807	-0.315	-0.875	-0.315
Fraction unbound (Fu)	0	0.26	0	0.109	0.296	0.414	0.354	0.414
BBB permeability (log BB)	-0.058	-1.074	-0.101	0.03	-1.124	-1.22	-1.083	-1.22
CNS permeability (log PS)	-2.134	-3.501	-2.16	-2.705	-0.739	-3.976	-3.798	-3.976
CYP2D6 substrate	No	No	No	No	No	No	No	No
CYP3A4 substrate	Yes	Yes	Yes	Yes	Yes	No	No	No
CYPC1A2 inhibitor	No	No	No	No	No	No	No	No
CYP2C19 inhibitor	No	No	No	No	No	No	No	No
CYP2C9 inhibitor	No	No	No	No	No	No	No	No
CYP2D6 inhibitor	No	No	No	No	No	No	No	No
CYP3A4 inhibitor	No	No	No	No	No	No	No	No
Total Clearance	-0.088	0.535	-0.04	0.425	0.564	0.5	0.638	0.5
Renal OCT2 substrate	No	No	No	Yes	No	No	No	No
AMES toxicity	No	No	No	No	No	No	No	No
Max. tolerated dose (log mg/kg/day)	-0.626	-1.653	-0.811	-0.758	-1.888	-2.207	-1.804	-2.207
hERG I inhibitor	No	No	No	No	No	No	No	No
hERG II inhibitor	Yes	Yes	No	No	Yes	Yes	Yes	Yes
Oral Rat Acute Toxicity (LD50) (mol/kg)	2.229	2.717	2.742	2.838	2.838	3.871	2.827	3.871
Oral Rat Chronic Toxicity (LOAEL) (log mg/kg_bw/day)	1.934	3.017	1.964	1.223	3.095	2.884	3.179	2.884
Hepatotoxicity	No	No	No	No	No	No	No	No
Skin Sensitisation	No	No	No	No	No	No	No	No
T.Pyriformis toxicity(log ug/L)	0.486	0.285	0.458	0.294	0.285	0.285	0.285	0.285
Minnow toxicity (log mM)	-1.144	2.232	-0.72	0.878	3.223	4.134	3.331	4.134

Another crucial factor during ADMET analysis was to predict the candidacy of compounds as non-substrates or inhibitors of P-glycoprotein, specifically P-glycoprotein I and II inhibitor11. All compounds, except daturaolone, were identified as a substrate for P-glycoprotein. Additionally, all compounds were found to be inhibitors of P-glycoprotein I. Three compounds are also observed to be P-glycoprotein II inhibitors except daturaturin A, daturametelin J, baimantuoluoside A, daturataurin B, and baimantuoluoside B (Table 4).

All the compounds were predicted to have Vdss lower than 0.71, which is considered to have a low distribution rate. Molecules with log BB values >0.3 are considered to readily cross the blood-brain barrier, while a log BB value <-1 indicates that the molecule is poorly

distributed. The range of log Ps <-2 to <-3 for CNS permeability indicated impenetrability [22]. None of the compounds were predicted to have the ability to cross the blood-brain barrier (BBB) or affect the central nervous system (CNS), except daturametelin J.

CYP450 enzymes are essential for drug metabolism in the liver [27]. The metabolism scores indicated that, except for daturaturin A, daturadiol, 12-deoxywithstramonolide, and daturametelin J, all the compounds were not substrates for CYP2D6 and CYP3A4. This suggests that daturaturin A, daturadiol, 12-deoxywithstramonolide, and daturametelin J may undergo biotransformation by the CYP3A enzyme, leading to the formation of metabolites that may be active or inactive. The reactive metabolite formed may pose a toxicity risk, according to Gleeson [28]. All the compounds also do not act as inhibitors for CYPC1A2, CYPsC19, CYP2C9, CYP2D6, and CYP3A4.

A combination of hepatic and renal clearance measures the total drug clearance. It is an important predictor for determining dosing rates to achieve steady-state concentrations. Total clearance quantifies the drug concentration within the body by utilizing the elimination rate, expressed as a log (ml/min/kg). The predicted results showed that the excretion of the compounds ranges from -0.088 to 0.638.

In drug discovery, toxicity is another crucial factor that plays a substantial role in the identification and selection of the most appropriate drug candidates [29]. All compounds are predicted to have a low maximum tolerated dose, suggesting that they are not well-tolerated at higher doses and may lead to undesirable and potentially harmful side effects. All the compounds displayed negative results for AMES toxicity tests, skin allergies, and hepatotoxic effects, which is a positive outcome in terms of safety. No inhibitory effects on hERG-I were observed for any of the compounds. However, daturaolone, daturataturin A, daturametelin J, baimantuoluoside A, daturataurin B, and baimantuoluoside B were predicted to be inhibitors of hERG-II. This suggests that these compounds have the capability to interact with the hERG channel, potentially leading to QT prolongation, a condition that can result in fatal cardiac arrhythmia [30].

4. Conclusions

To the best of our knowledge, this is the first *in silico* study to describe the inhibitory effects of Datura fastuosa against M*pro*. In this research study, the bioactive compounds in *Datura fastuosa* were subjected to several experiments, such as molecular docking, Lipinski's rule of five, chemical interaction evaluation, and ADMET analysis, with M^{pro} as the protein target of SARS-CoV-2. As M^{pro} plays an important role in the replication of the virus, the inhibition of this enzyme can diminish the spread of the illness. Our docking results predicted that daturataturin A, daturametelin J, baimantuoluoside A, baimantuoluoside B, 12-deoxywithastramonolide, daturaolone, daturadiol, and daturataurin B are exclusive compounds from *Datura fastuosa* that exhibit higher binding efficacy with M^{pro} than the positive control, N3 inhibitor. However, these compounds still display shortcomings in terms of predicted drug-likeness and ADMET properties. Consequently, further investigation is needed to determine the efficacy and safety of *Datura fastuosa* compounds *in vivo* and *in vitro* settings. Nevertheless, due to their high binding affinities, these compounds remain promising candidates for potential drug development, serving as valuable templates for future research for SARS-CoV-2.

Funding

This research was funded by the Ministry of Higher Education (MoHE) Malaysia through the Fundamental Research Grant Scheme (FRGS/1/2020/SKK0/TAYLOR/02/2).

Acknowledgments

This work was supported by the School of Biosciences, Faculty of Health and Medical Sciences, Taylor's University, Malaysia.

Conflicts of Interest

The authors declare no conflict of interest.

References

1. Ng, T.I.; Correia, I.; Seagal, J.; DeGoey, D.A.; Schrimpf, M.R.; Hardee, D.J.; Noey, E.L.; Kati, W.M. Antiviral Drug Discovery for the Treatment of COVID-19 Infections. *Viruses* **2022**, *14*, 961, https://doi.org/10.3390/v14050961.
2. Ciotti, M.; Ciccozzi, M.; Terrinoni, A.; Jiang, W.-C.; Wang, C.-B.; Bernardini, S. The COVID-19 pandemic. *Crit. Rev. Clin. Lab. Sci.* **2020**, *57*, 365-388, https://doi.org/10.1080/10408363.2020.1783198.
3. Organization, W.H. WHO Coronavirus (COVID-19) Dashboard. Available online: https://covid19.who.int/ (accessed on 29 March).
4. Roe, M.K.; Junod, N.A.; Young, A.R.; Beachboard, D.C.; Stobart, C.C. Targeting novel structural and functional features of coronavirus protease nsp5 (3CL^{pro}, M^{pro}) in the age of COVID-19. *J. Gen. Virol.* **2021**, *102*, 001558, https://doi.org/10.1099/jgv.0.001558.
5. Liu, X.; Wang, X.-J. Potential inhibitors against 2019-nCoV coronavirus M protease from clinically approved medicines. *J. Genet. Genom.* **2020**, *47*, 119-121, https://doi.org/10.1016/j.jgg.2020.02.001.
6. Chun, C.Y.; Khor, S.X.Y.; Chia, A.Y.Y.; Tang, Y.-Q. *In silico* study of potential SARS-CoV-2 antagonist from *Clitoria ternatea*. *Int. J. Health Sci.* **2023**, *17*, 3-10.
7. Zhang, L.; Lin, D.; Sun, X.; Curth, U.; Drosten, C.; Sauerhering, L.; Becker, S.; Rox, K.; Hilgenfeld, R. Crystal structure of SARS-CoV-2 main protease provides a basis for design of improved α-ketoamide inhibitors. *Science* **2020**, *368*, 409-412, https://doi.org/10.1126/science.abb3405.
8. Al-Snafi, A.E. Medical importance of *Datura fastuosa* (syn: *Datura metel*) and Datura stramonium - A review. *IOSR J. Pharm.* **2017**, *7*, 43-58, http://dx.doi.org/10.9790/3013-0702014358.
9. Lipinski, C.A.; Lombardo, F.; Dominy, B.W.; Feeney, P.J. Experimental and computational approaches to estimate solubility and permeability in drug discovery and development settings. *Adv. Drug Deliv. Rev.* **2001**, *46*, 3-26, https://doi.org/10.1016/s0169-409x(00)00129-0.
10. Dey, D.; Hossain, R.; Biswas, P.; Paul, P.; Islam, M.A.; Ema, T.I.; Gain, B.K.; Hasan, M.M.; Bibi, S.; Islam, M.T.; Rahman, M.A.; Kim, B. Amentoflavone derivatives significantly act towards the main protease (3CL^{PRO}/M^{PRO}) of SARS-CoV-2: in silico admet profiling, molecular docking, molecular dynamics simulation, network pharmacology. *Mol. Diver.* **2023**, *27*, 857-871, https://doi.org/10.1007/s11030-022-10459-9.
11. Padmi, H.; Kharisma, V.D.; Ansori, A.N.M.; Sibero, M.T.; Widyananda, M.H.; Ullah, E.; Gumenyuk, O.; Chylichcova, S.; Bratishko, N.; Prasedya, E.S. Macroalgae Bioactive Compounds for the Potential Antiviral of SARS-CoV-2: An *In Silico* Study. *J. Pure Appl. Microbiol.* **2022**, *16*, 1018-1027, https://doi.org/10.22207/JPAM.16.2.26.
12. Ferreira, J.C.; Fadl, S.; Villanueva, A.J.; Rabeh, W.M. Catalytic Dyad Residues His41 and Cys145 Impact the Catalytic Activity and Overall Conformational Fold of the Main SARS-CoV-2 Protease 3-Chymotrypsin-Like Protease. *Front. Chem.* **2021**, *9*, 692168, https://doi.org/10.3389/fchem.2021.692168.
13. Lim, J.Y.; Gew, L.T.; Tang, Y.-Q. Biocomputational-mediated screening and molecular docking platforms for discovery of coumarin-derived antimelanogenesis agents. *Dermatol. Sin.* **2023**, *41*, 8-17, https://doi.org/10.4103/ds.DS-D-22-00087.

14. Patil, R.; Das, S.; Stanley, A.; Yadav, L.; Sudhakar, A.; Varma, A.K. Optimized Hydrophobic Interactions and Hydrogen Bonding at the Target-Ligand Interface Leads the Pathways of Drug-Designing. *PloS ONE* **2010**, *5*, e12029, https://doi.org/10.1371/journal.pone.0012029.
15. Hao Dong, T.; Yau Wen Ning, A.; Yin Quan, T. Network pharmacology-integrated molecular docking analysis of phytocompounds of *Caesalpinia pulcherrima* (peacock flower) as potential anti-metastatic agents. *J. Biomol. Struct. Dyn.* **2024**, *42*, 1778-1794, https://doi.org/10.1080/07391102.2023.2202273.
16. Bhat, R.A.H.; Tandel, R.S.; Dash, P.; Nazir, M.I.; Yousuf, D.J.; Bhat, I.A.; Ganie, P.A.; Gargotra, P.; Siva, C. Computational analysis and functional characterisation of *Tor putitora* toll-like receptor 4 with the elucidation of its binding sites for microbial mimicking ligands. *Fish Shellfish Immunol.* **2022**, *130*, 538-549, https://doi.org/10.1016/j.fsi.2022.09.046.
17. Fu, Y.; Zhao, J.; Chen, Z. Insights into the Molecular Mechanisms of Protein-Ligand Interactions by Molecular Docking and Molecular Dynamics Simulation: A Case of Oligopeptide Binding Protein. *Comput. Math. Methods Med.* **2018**, *2018*, 3502514, https://doi.org/10.1155/2018/3502514.
18. Yow Hui, Y.; Tang, Y.-Q. Computational Screening of Repurposed Drugs Targeting Sars-Cov-2 Main Protease By Molecular Docking. *Sudan J. Med. Sci.* **2022**, *17*, 387–400, https://doi.org/10.18502/sjms.v17i3.12125.
19. Abbas, N.; Tan, H.D.; Goh, B.-H.; Yap, W.H.; Tang, Y.-Q. In *Silico* Study of Anticancer and Antimicrobial Peptides Derived from Cycloviolacin O2 (CyO2). *Biointerface Res. Appl. Chem.* **2023**, *13*, 437, https://doi.org/10.33263/BRIAC135.437.
20. Lipinski, C.A. Rule of five in 2015 and beyond: Target and ligand structural limitations, ligand chemistry structure and drug discovery project decisions. *Adv. Drug Deliv. Rev.* **2016**, *101*, 34-41, https://doi.org/10.1016/j.addr.2016.04.029.
21. Wijaya, R.M.; Hafidzhah, M.A.; Kharisma, V.D.; Ansori, A.N.M.; Parikesit, A.A. COVID-19 *In Silico* Drug with *Zingiber officinale* Natural Product Compound Library Targeting the M^{pro} Protein. *Makara J. Sci.* **2021**, *25*, 162-171, https://doi.org/10.7454/mss.v25i3.1244.
22. Pires, D.E.V.; Blundell, T.L.; Ascher, D.B. pkCSM: Predicting Small-Molecule Pharmacokinetic and Toxicity Properties Using Graph-Based Signatures. *J. Med. Chem.* **2015**, *58*, 4066-4072, https://doi.org/10.1021/acs.jmedchem.5b00104.
23. Dahlgren, D.; Lennernäs, H. Intestinal Permeability and Drug Absorption: Predictive Experimental, Computational and In Vivo Approaches. *Pharmaceutics* **2019**, *11*, 411, https://doi.org/10.3390/pharmaceutics11080411.
24. Savjani, K.T.; Gajjar, A.K.; Savjani, J.K. Drug Solubility: Importance and Enhancement Techniques. *ISRN Pharm.* **2012**, *2012*, 195727.
25. Pouton, C.W. Formulation of poorly water-soluble drugs for oral administration: physicochemical and physiological issues and the lipid formulation classification system. *Eur. J. Pharm. Sci.* **2006**, *29*, 278-287, https://doi.org/10.1016/j.ejps.2006.04.016.
26. Murugesan, S.; Kottekad, S.; Crasta, I.; Sreevathsan, S.; Usharani, D.; Perumal, M.K.; Mudliar, S.N. Targeting COVID-19 (SARS-CoV-2) main protease through active phytocompounds of ayurvedic medicinal plants - *Emblica officinalis* (Amla), *Phyllanthus niruri* Linn. (Bhumi Amla) and *Tinospora cordifolia* (Giloy) - A molecular docking and simulation study. *Comput. Biol. Med.* **2021**, *136*, 104683, https://doi.org/10.1016/j.compbiomed.2021.104683.
27. Zanger, U.M.; Schwab, M. Cytochrome P450 enzymes in drug metabolism: regulation of gene expression, enzyme activities, and impact of genetic variation. *Pharmacol. Ther.* **2013**, *138*, 103-141, https://doi.org/10.1016/j.pharmthera.2012.12.007.
28. Gleeson, M.P. Generation of a Set of Simple, Interpretable ADMET Rules of Thumb. *J. Med. Chem.* **2008**, *51*, 817-834, https://doi.org/10.1021/jm701122q.
29. Han, Y.; Zhang, J.; Hu, C.Q.; Zhang, X.; Ma, B.; Zhang, P. *In silico* ADME and Toxicity Prediction of Ceftazidime and Its Impurities. *Front. Pharmacol.* **2019**, *10*, 434, https://doi.org/10.3389/fphar.2019.00434.
30. Zhao, J.; Xia, M. Cell-Based hERG Channel Inhibition Assay in High-Throughput Format. In *High-Throughput Screening Assays in Toxicology*, Zhu, H., Xia, M., Eds.; Springer US: New York, NY, **2022**; Volume 2474, 21-28, https://doi.org/10.1007/978-1-0716-2213-1_3.